Membrane Lateral Diffusion and Capture of CFTR within Transient Confinement Zones

Ian R. Bates,* Benedict Hébert,‡ Yishan Luo,* Jie Liao,* Alexia I. Bachir,† David L. Kolin,† Paul W. Wiseman,†‡ and John W. Hanrahan*
Departments of *Physiology, †Chemistry, and ‡Physics, McGill University, Montréal, Québec, Canada H3G 1Y6

ABSTRACT The cystic fibrosis transmembrane conductance regulator (CFTR) channel interacts with scaffolding and other proteins that are expected to restrict its lateral movement, yet previous studies have reported predominantly free diffusion. We examined the lateral mobility of CFTR channels on live baby hamster kidney cells using three complementary methods. Channels bearing an extracellular biotinylation target sequence were labeled with streptavidin conjugated with fluorescent dyes (Alexa Fluor 488 or 568) or quantum dots (qDot605). Fluorescence recovery after photobleaching and image correlation spectroscopy of the dye-labeled channels revealed a significant immobile population (~50%), which was confirmed by direct single particle tracking (SPT) of qDot605-labeled CFTR. Adding 10 histidine residues at the C-terminus of CFTR to mask the postsynaptic density 95, Discs large, ZO-1 (PDZ) binding motif abolished its association with EBP50/NHERF1, reduced the immobile fraction, and increased mobility. Other interactions that are not normally detected on this timescale became apparent when binding of PDZ domain proteins was disrupted. SPT revealed that $CFTR_{His\text{-}10}$ channels diffuse randomly, become immobilized for periods lasting up to 1 min, and in some instances are recaptured at the same location. The impact of transient confinement on the measured diffusion using the three fluorescence techniques were assessed using computer simulations of the biological experiments. Finally, the impact of endosomal CFTR on mobility measurements was assessed by fluorescence correlation spectroscopy. These results reveal unexpected features of CFTR dynamics which may influence its ion channel activity.

INTRODUCTION

The cystic fibrosis transmembrane conductance regulator (CFTR) is an anion channel which mediates cAMP-stimulated chloride conductance in epithelial and other cell types and is defective in the genetic disease cystic fibrosis (1). CFTR is regulated by phosphorylation and by interactions with proteins such as EBP50 (ezrin binding protein of 50 kDa, also known as sodium-hydrogen exchange regulatory factor or NHERF). EBP50 is an adaptor protein that is critical for the organization of receptors and channels and is expressed at the apical membranes of many polarized epithelial cells (2). Interactions of CFTR through its carboxyl terminal consensus motif for PDZ (postsynaptic density 95, Discs large, ZO-1) domains (3) may influence the apical membrane targeting and regulation of CFTR (4,5). CFTR channel activity also depends on associations with the t-SNARE syntaxin 1A (6) and may be regulated by the actin cytoskeleton (7) and a wide range of channels and transporters (8). Interaction with other proteins is expected to slow CFTR diffusion in the membrane, yet most CFTR-GFP fusion proteins in previous studies were mobile (9,10) and the determinants of CFTR lateral mobility remain poorly understood.

The goals of this study were to 1), measure the lateral mobility of wild-type CFTR, 2), investigate the importance of the PDZ domain in channel dynamics, and 3), compare three methods for determining the diffusion coefficients of a membrane protein under the same experimental conditions: fluorescence recovery after photobleaching (FRAP), image correlation spectroscopy (ICS), and single particle tracking (SPT). We used baby hamster kidney (BHK) cells stably expressing CFTR with an extracellular biotinylation target sequence and labeled the channels with streptavidin conjugated to fluorescent dyes or quantum dots (qDot). An extracellular tag was used to preserve interactions between the cytoplasmic domains of CFTR and intracellular proteins and to avoid background fluorescence from intracellular GFP fusion protein.

With FRAP, the diffusion coefficient is calculated from the rate at which a small bleached area of the sample becomes repopulated by fluorescent molecules (11). In ICS, the diffusion coefficient is calculated from fluorescence intensity fluctuations in a time series of confocal images (12). Since the fluctuations are analyzed from many pixels simultaneously, ICS is better suited for studying slow diffusion in membranes than conventional fluorescence correlation spectroscopy (FCS). SPT also yields the diffusion coefficient and enables the analysis of more complex behaviors than ensemble methods. It is of considerable interest to compare the results obtained in live cells using these very different methods. In this study, FRAP consistently yielded a higher diffusion coefficient than ICS. However SPT revealed the presence of transient confinement zones, and computer simulations revealed that the different diffusion

Submitted March 10, 2006, and accepted for publication May 8, 2006.

Address reprint requests to John W. Hanrahan, PhD, Dept. of Physiology, McGill University, 3655 Promenade Sir William Osler, Rm. 1012, Montréal, Québec, Canada H3G 1Y6. E-mail: john.hanrahan@mcgill.ca.

0006-3495/06/08/1046/13 $2.00

doi: 10.1529/biophysj.106.084830

coefficients could be explained by a lower sensitivity of FRAP to confinement.

Wild-type CFTR diffused slowly and had a large immobile fraction (>50%) according to ICS and FRAP. At the single molecule level, CFTR-bound qDots were nearly stationary; however when a decahistidine tag was added at the C-terminus of CFTR ($CFTR_{His\text{-}10}$) to disrupt its binding to EBP50, lateral mobility increased and the immobile fraction was reduced. Interestingly, $CFTR_{His\text{-}10}$ channels diffused rapidly but were occasionally captured for periods lasting up to a minute, which may reflect temporary interactions with other protein partners or trapping within lipid domains. We conclude that most wild-type CFTR is tethered by its C-terminus, which has profound implications for the regulation of CFTR channels in epithelial cells. Rapid diffusion and transient interactions after release from PDZ proteins would help explain how CFTR channels interact with many different protein partners.

MATERIALS AND METHODS

cDNA constructs and transfections

Nucleotides encoding a biotinylation target sequence comprising 15 amino acids (13) were inserted into the fourth extracellular loop of pNUT-CFTR and pNUT-$CFTR_{His\text{-}10}$ after amino acid 901, a site which is known to tolerate insertion of an antibody epitope (14). The plasmid was transfected into BHK cells by calcium phosphate coprecipitation, and stable lines were selected using 500 μM methotrexate as described previously (15). Although the efficiency of CFTR trafficking to the cell surface was reduced slightly by the biotinylation sequence, Western blotting revealed a strong ''band C'' that is indicative of complex glycosylated (mature) protein, and CFTR function was confirmed by measuring cAMP-stimulated iodide effluxes and by single channel recording. Details of the construction and functionality of CFTR-biotintag will be presented elsewhere. Unless otherwise noted, all chemicals were obtained from Sigma-Aldrich (St. Louis, MO).

Cloning and purification of BirA from *E. coli*

The biotin ligase BirA was cloned from *Escherichia coli* and expressed as a glutathione-S-transferase (GST) fusion protein as described previously (16). A single colony of BL21-codon plus cells that had been transformed with PET vector containing BirA-GST was cultured in Ampicillin (100 μg/ml) to optical density 600 = 0.6–1.0, induced with 0.5 M isopropyl-β-D-thiogalactoside (IPTG), lysed by sonication, and centrifuged at 7000 × g. The supernatant was incubated with glutathione sepharose beads overnight at 4°C, which were subsequently washed and incubated overnight with 50 μg thrombin at 4°C to release BirA. The purified biotin ligase was eluted in phosphate buffer saline (PBS) and stored at 4°C for up to 2 months.

Purification and pulldown of CFTR and $CFTR_{His\text{-}10}$ using the biotin tag

After exposure to BirA, cells in a 65-mm culture dish were rinsed three times with PBS and solubilized for 15 min at 4°C in radioimmunoprecipitation (RIPA) buffer (150 mM NaCl, 1 mM Tris-Cl, 1% deoxycholic acid (w/v), 1% Triton X-100 (w/v), and 0.1% sodium dodecyl sulfate (SDS)) containing protease inhibitors. The lysate was centrifuged (32,000 × g, 15 min, 4°C), and the supernatant was incubated at 4°C for 2 h with 25 μL streptavidin beads (preequilibrated with RIPA buffer) and briefly centrifuged. The supernatant was removed and an aliquot run on an SDS- polyacrylamide gel electrophoresis (PAGE) gel for Western blot analysis of unbound (i.e., unbiotinylated) CFTR-biotintag. Beads were washed five times with RIPA buffer, and adsorbed proteins were eluted by boiling for 3 min, centrifuged briefly, and loaded on an SDS-PAGE gel. Proteins were transferred to polyvinylidene fluoride membranes, and Western blots were performed with anti-R domain monoclonal antibody at 1:5000 dilution, or anti-NHERF1 polyclonal antibody (Chemicon, Mississauga, Canada) at 1:500 dilution.

Enzymatic biotinylation and fluorescent labeling of CFTR

BHK cells were plated in four-well Lab-Tek chambers (Nalge Nunc, Naperville, IL) for live cell imaging and on sterile coverslips for studies of fixed preparations and cultured to 70% confluence in Dulbecco's modified Eagle's medium(DMEM)-F12 supplemented with 10% fetal bovine serum and 500 μg methotrexate. CFTR-biotintag on the cell surface was enzymatically biotinylated by exposure to PBS supplemented with 50 mM bicine (pH 8.3), 10 mM magnesium acetate, 10 mM ATP, 400 μM biotin, and 5 μg biotin ligase for 40–60 min at 30°C. Cells were then incubated with 2% BSA in medium for 30 min at 16°C to block nonspecific binding and labeled with fluorescent dye by exposure to 10 μg of streptavidin conjugated with Alexa Fluor 488 or Alexa Fluor 568 (Molecular Probes, Eugene, OR) in PBS for 30 min on ice (Fig. 1 *a*). After washing off excess fluorophore with cold DMEM-F12, cells were placed on the microscope stage and warmed to 23°C or 37°C for imaging (FCS2, Bioptechs, Butler, PA).

Fluorescence recovery after photobleaching

FRAP was performed using a confocal microscope (LSM 510META; Carl Zeiss Microimaging, Thornwood, NY) with a 63× objective (numerical aperture (NA) 1.4) and pinhole set to 1–2 Airy units. Streptavidin-Alexa 488 was excited using the 488-nm line of a 30-mW Kr/Ar laser. Five prebleach measurements of fluorescence intensity were taken using 1% laser power after which a 2–5-μm-wide strip was photobleached for <1 s using 75% laser power. Recovery of fluorescence within the strip was continually imaged at low laser power (1%) with a 4–5-s interval between frames until fluorescence reached a steady-state plateau. Diffusion coefficients were determined using Diffuse, a program kindly provided by Dr. Eric Siggia (17) which models diffusive recovery into the bleached region using the postbleach image series. Image series were analyzed with Diffuse on the Clumeq supercomputer cluster (McGill University, Montréal, QC). The immobile fraction (IM_f) of CFTR was calculated by standard FRAP methods as described previously (18).

Image correlation spectroscopy

To study lateral diffusion of biotinylated CFTR using ICS, cells were exposed to Streptavidin-Alexa 568 at 4°C, washed, and rewarmed to 23°C or 37°C in the incubation chamber on the microscope stage. Images were collected after excitation with the 543-nm line of a 1-mW He-Ne laser using the LSM 510META and filter sets supplied by Zeiss. Fluorescence emitted by Streptavidin-Alexa 568 was collected using a 63× PlanApo oil immersion objective (NA 1.4) with the confocal pinhole set at 1 Airy unit. Individual cells were viewed using an electronic zoom, which gave a pixel size of between 0.06 and 0.15 μm/pixel in the x and y directions. Time series of 100–125 images were collected, with ~1 s between each scanned image. Control experiments were performed with biotinylated cells that had been prefixed by exposure to 2% paraformaldehyde in PBS for 20 min at room temperature. A subregion of 32 × 32 pixels was selected from the image series for temporal ICS analysis. The normalized spatiotemporal intensity fluctuation autocorrelation function was defined as (12)

$$r(\zeta,\eta,\tau)=\frac{\langle \delta i(x+\zeta,y+\eta,t+\tau)\delta i(x,y,t)\rangle}{\langle i\rangle^2}, \qquad (1)$$

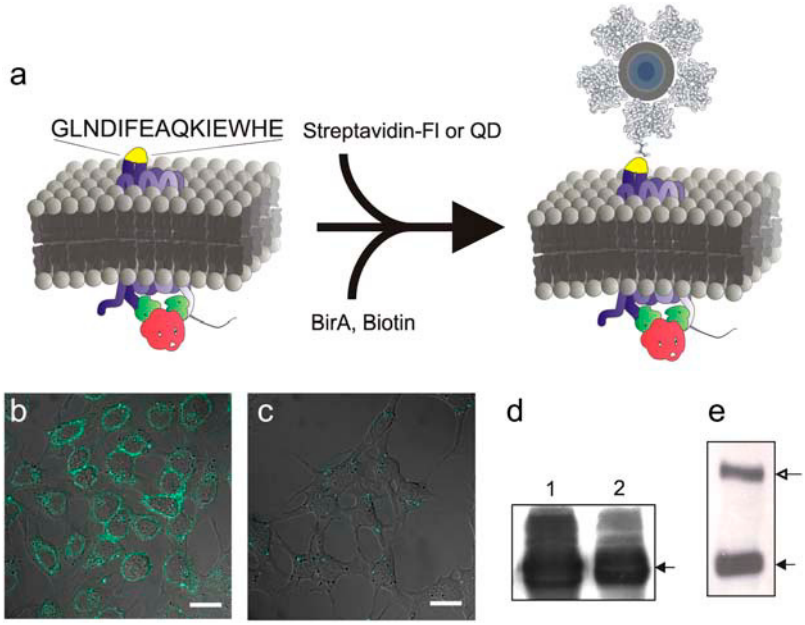

FIGURE 1 Expression and labeling of CFTR on live BHK cells. (*a*) Diagram illustrating the enzymatic biotinylation of CFTR on the cell surface. (*b* and *c*) Low magnification fluorescence images of BHK cells stably expressing CFTR-biotintag. (*b*) Cells were exposed to the biotin ligase BirA for 40 min at 30°C and incubated with Streptavidin-Alexa Fluor 488. (*c*) In the absence of BirA, there was little nonspecific binding. Scale bar, 20 μm. (*d*) Western blot of wild-type His tagged CFTR purified using Ni^{2+}-NTA beads (48) (*lane 1*) and CFTR-biotintag (*lane 2*). Arrow indicates location of standard at 175 kDa. (*e*) Western blot of CFTR-biotintag after incubation with streptavidin. Solid arrow indicates the monomeric, complex-glycosylated protein at 175 kDa. The open arrow indicates 350 kDa dimers stabilized by streptavidin pretreatment.

where ζ and η are the spatial lag variables in the x and y directions, and τ is the time lag variable between correlated pairs of images. By setting the temporal lag to zero, spatial autocorrelation functions were calculated for each image in the time series and fitted to a Gaussian function by nonlinear least-squares fitting (12):

$$r(\zeta,\eta,0) = g(0,0,0)_{\mathrm{n}} e^{-(\zeta^2+\eta^2)/\omega_{\mathrm{n}}^2} + g_{\mathrm{n}\infty}, \qquad (2)$$

where the fitting parameters for the ''n^{th}'' image are the zero lags spatial autocorrelation function amplitude $g(0,0,0)_{\mathrm{n}}$, the e^{-2} beam radius in the focal plane ω_{n}, and an offset parameter at long correlation lengths $g_{\mathrm{n}\infty}$. By setting the spatial lag variables to zero, a temporal autocorrelation function was calculated for each time series and fit to a two-dimensional (2D) diffusion model (12):

$$r(0,0,\tau) = g(0,0,0)\left(1+\frac{\tau}{\tau_{\mathrm{d}}}\right)^{-1} + g_{\mathrm{t}\infty}, \qquad (3)$$

where the fitting parameters are the zero lag temporal autocorrelation function amplitude $g(0,0,0)$, the characteristic diffusion time τ_{d}, and an offset parameter at long correlation times $g_{\mathrm{t}\infty}$.

For each image time series, a diffusion coefficient was calculated using the average value of the best-fit beam radii from the spatial autocorrelation function fits ($\langle\omega\rangle$) and the recovered characteristic diffusion time:

$$D = \frac{\langle\omega\rangle^2}{4\tau_{\mathrm{d}}}. \qquad (4)$$

The immobile fraction was calculated using the amplitude and offset of the temporal autocorrelation function as has been described (19):

$$\%\mathrm{Immobile} = \frac{g_{\mathrm{t}\infty}}{g_{\mathrm{t}\infty} + g(0,0,0)} \times 100. \qquad (5)$$

All correlation calculations and fitting of spatial autocorrelation functions were performed using programs written in the IDL programming language (Interactive Data Language, RSI, Boulder, CO).

Fluorescence correlation spectroscopy

FCS was performed on a ConfoCor2/LSM combination system (Zeiss, Jena, Germany), using the autocorrelation configuration. The 488-nm line of an Argon-Krypton laser line was attenuated to 15 μW using an acousto-optical filter, and a 488 beam splitter reflected the light which was focused through a Zeiss C-Apochromat 40×, NA 1.2 water immersion objective onto the sample. The fluorescence emission was passed through a 505–550-nm bandpass and detected using avalanche photodiodes and a pinhole diameter of 70 μm. The fluorescence signal was recorded for 3–5 consecutive periods of 10 s. The signal was displayed online, and the autocorrelation function and data fitting were performed with the appropriate model in the ConfoCor2 software using a one- or two-component fit (Zeiss). The lateral radius (ω) of the detection volume was found to be ~0.15 μm with a calibration using the known diffusion coefficient of Rhodamine-6G at room temperature (2.8 $\mu m^2 s^{-1}$). Intracellular measurements were done by positioning the confocor focal volume at the membrane of an individual cell while monitoring via LSM imaging. The appropriate z-focus was determined by doing a z-scan through the membrane.

Single particle tracking

Biotinylated cells were exposed to Tyrode's buffer containing 0.02 nmoles streptavidin-qDot605 (Quantum Dot, Hayward, CA), 0.1 nmoles free biotin, and 2.5% BSA at 4°C. Cells were then washed and rewarmed in the incubation chamber, and the confocal image time series were collected at 2–20 Hz using excitation with the 488-nm laser line of a 30-mW Kr/Ar ion laser and filter sets recommended by Quantum Dot Corp. The image series were analyzed using SPT programs to track the trajectories of individual nanoparticles (~15 nm diameter) attached to cell surface CFTR channels. Nanoparticles that were not bound to cell membrane components and were diffusing freely in solution moved too quickly to be resolved at this imaging rate and thus did not perturb the SPT measurements. Particle trajectories were analyzed to calculate mean-squared displacement (MSD) versus time curves, which were fit to calculate diffusion coefficients using standard SPT methods (20). The images were first processed using a spatial bandpass filter to smooth the images and subtract background fluorescence. Coordinates of the resolved intensity spots in the filtered image were determined by locating their centroids using both intensity and eccentricity of the spots as rejection criteria when discriminating real features from noise. Given the positions for ''n'' particles at time $t(i)$ and ''m'' possible new positions at time $t(i+1)$, we considered all possible identifications of ''n'' old and ''m'' new positions and chose the result that minimized the overall squared displacement. This algorithm yields the most likely set of identifications for noninteracting

Brownian particles having the same diffusivity and works well for systems with oscillatory, ballistic, correlated, or random hopping motions when the single time step displacements are relatively small. Transient confinement zones were defined as regions where the local mean-square displacement falls below a preset threshold (21). All SPT calculations and fitting were performed using programs written in IDL.

Computer simulations

Computer simulations were used to model the expected results for different channel transport properties and measurement conditions to allow direct comparison with the experimental results. An IDL program was written to simulate, as closely as possible, the ICS and FRAP data that would be obtained by laser scanning microscopy of point emitters in a 2D system under defined settings of instrument collection and particle mobility. Simulation of confinement was based on Wawrezinieck et al. (22), where the probability for entering and exiting domains of defined size can be assigned (probability in (P_{in}), probability out (P_{out})) as well as the diffusion coefficient inside and outside of the domains (diffusion in (D_{in}), diffusion out (D_{out})). The program allowed many system parameters to be varied, including characteristic diffusion times, densities of particle populations, laser beam size and shape characteristics, size of hypothetical confinement areas, image size, pixel size, the number of images collected for analysis, the time interval between images, and the emission state of every particle (''on'' or ''off''). For FRAP simulations, a prebleach image was created in which all the particles were emitting (''on''), then a thin strip of variable width and height was ''bleached'' by setting all of the particles in that region to be in the ''off'' state (irreversible bleaching), and the postbleach image sequence was then simulated. Periodic boundary conditions were used at the image edges, and discrete displacements in x and y were computed at every time step for each particle using normally distributed, floating-point, pseudorandom numbers having a mean of zero and standard deviation $\sigma = \sqrt{2Dt}$. The simulations were run on a standard desktop PC.

RESULTS

Labeling of CFTR on the cell surface

After insertion of the biotinylation target sequence, CFTR could be enzymatically biotinylated and specifically labeled with a variety of streptavidin conjugates (Fig. 1 *a*). In the presence of BirA, distinct membrane staining of CFTR on the cell surface was observed (Fig. 1 *b*), whereas in the absence of BirA the fluorescence was not detected (Fig. 1 *c*). CFTR was trafficked correctly and not trapped in the endoplasmic reticulum as indicated by the mature, complex glycosylated band C form in Western blots (Fig. 1 *d*). In addition, it was found that some CFTR molecules could be cross-linked by the addition of streptavidin (Fig. 1 *e*), although this may reflect stabilization of a naturally occurring dimer that exists natively in the membrane (23) (see ''Cross-linking'' section below).

Most CFTR appears immobilized on the cell surface

FRAP was performed on cells labeled with Streptavidin-Alexa 488 that was bound to biotinylated CFTR. To minimize endocytosis of labeled CFTR (24), experiments were performed within the first 30 min after warming of the cells in the incubation chamber on the microscope. As expected, fluorescence was localized on the cell surface when living cells were viewed in optical cross sections on the confocal microscope. Reversible photobleaching was not detected using control cells prefixed with 2% paraformaldehyde (data not shown). The immobile fraction (IM_f) was calculated as described (18) after correcting for the background and for fluorescence loss over the course of the measurement (Fig. 2 *b*). The IM_f was found to be on average 50% ± 8%, and a typical FRAP recovery curve for wild-type CFTR is shown in Fig. 2 *c*. The large immobile fraction precluded fitting of the diffusive recovery within the bleached region to determine the diffusion coefficient (17).

To study channel mobility using ICS, confocal images of cells labeled with Streptavidin-Alexa 568 that was bound to biotinylated CFTR were collected at 1-s intervals, and the intensity fluctuations in a 32 × 32 pixel subregion time stack were analyzed. A typical en face image used for analysis is shown in Fig. 2 *a* along with the discrete autocorrelation function calculated from a time series of >100 frames (Fig. 2 *e*). Superimposed on the autocorrelation function is the best-fit solid line obtained using a 2D diffusion model (see Eq. 3). The τ_d obtained by this method yields an average diffusion coefficient $D = 8.0 \pm 2.7 \times 10^{-4}\ \mu m^2 s^{-1}$ and an immobile fraction of 41% ± 8%, indicating that a significant fraction of CFTR molecules are essentially immobile in the cell membrane ($N = 18$ cells).

Lateral mobility of $CFTR_{His\text{-}10}$ on the cell surface

$CFTR_{His\text{-}10}$ was used to determine the effect of interfering with the PDZ domain binding on CFTR mobility. Western blot analysis of a pulldown using the biotinylation target sequence and avidin agarose beads showed that the 10His tag prevents the binding of EBP50 to the C-terminus of $CFTR_{His\text{-}10}$ (Fig. 3, *a–c*). The immobile fraction of $CFTR_{His\text{-}10}$ measured by FRAP was found to be on average 22% ± 14% ($N = 28$ cells), and a typical FRAP recovery curve is shown in Fig. 2 *d*. The resulting time-course was analyzed by assuming diffusive entry into the bleached strip (17). The values for diffusion coefficient were similar at room temperature ($1.4 \pm 0.6 \times 10^{-2}\ \mu m^2 s^{-1}$) and at 37°C ($1.5 \pm 0.5 \times 10^{-2}\ \mu m^2 s^{-1}$).

ICS analysis of $CFTR_{His\text{-}10}$ yielded a diffusion coefficient of $D = 3.8 \pm 1.7 \times 10^{-3}\ \mu m^2 s^{-1}$ (Fig. 2 *f*) at room temperature, ~4-fold slower than that obtained by FRAP. Again, similar diffusion coefficients were obtained at 37°C ($4.1 \pm 1.2 \times 10^{-3}\ \mu m^2 s^{-1}$). The immobile fraction estimated from the best-fit temporal offset parameter $g_{t\infty}$ was 28% ± 10%.

Single particle tracking and ICS studies of CFTR on the cell surface using quantum dots

SPT can yield detailed information about lateral movements of single molecules that cannot be obtained by ensemble analysis of populations using FRAP or ICS (25). We took

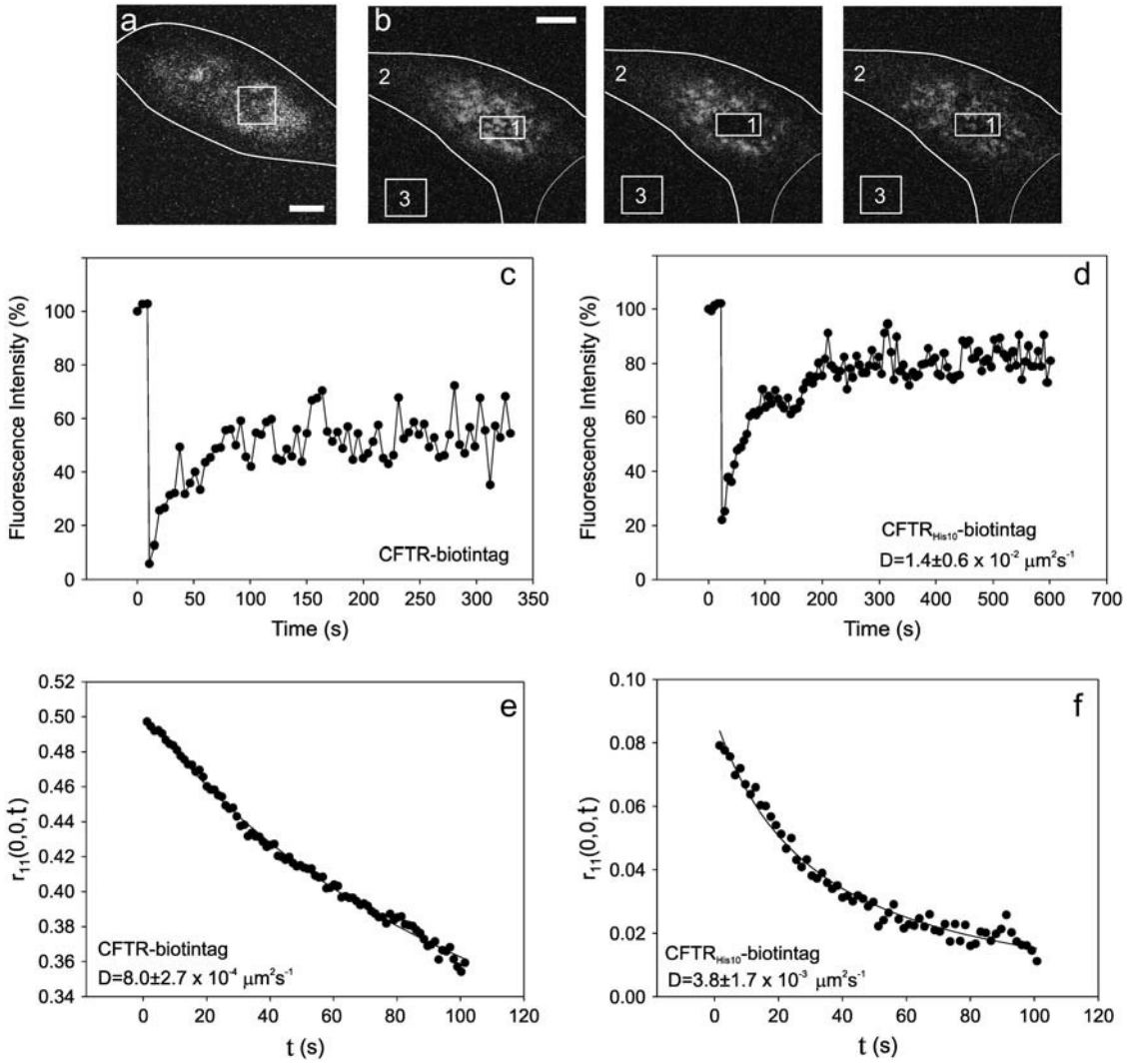

FIGURE 2 Distribution and lateral mobility of biotinylated CFTR and CFTR$_{His-10}$ studied by FRAP and ICS. (*a*) High magnification image of the upper surface of a labeled cell. The white square indicates a 32 × 32 pixel area that was analyzed to produce a stack of 100 consecutive images collected at 1–2-s intervals. Scale bar, 5 μm. (*b*) Selected images from a confocal FRAP experiment at 37°C of CFTR-biotintag labeled with Streptavidin-Alexa Fluor 488 expressed in BHK cells. Nos. 1–3 represent the bleach box, whole cell fluorescence, and background fluorescence, respectively. Bleach box length, 5 μm. Scale bar, 4 μm. (*c* and *d*) Fluorescence recovery kinetics for CFTR (*c*) and CFTR$_{His-10}$ (*d*). Note the smaller immobilized fraction with CFTR$_{His-10}$. (*e* and *f*) Normalized temporal intensity fluctuation autocorrelation function from CFTR (*e*) and CFTR$_{His-10}$ (*f*) with solid line curve of best fit to the 2D diffusion model (see Materials and Methods). Representative of 20 cells imaged on different days.

advantage of the favorable photophysical properties of quantum dots, namely their brightness and resistance to photobleaching (26), to perform SPT studies of CFTR on the cell surface and compared the results with those obtained by ICS. The upper surface of the cell was imaged at various scan speeds (2–20 Hz), and the trajectories of the quantum dot-CFTR complexes were tracked in the image time series by SPT. The trajectories were analyzed to calculate MSD versus time curves, which were fit to determine diffusion coefficients for the nanoparticle-channel complexes.

We imaged the dynamics of both CFTR and CFTR$_{His-10}$ at the single nanoparticle level and observed several behaviors (see Supplementary Material for movies). CFTR was essentially immobilized as measured by SPT, and this was stable throughout the experiment (see Movie 1). By contrast, most CFTR$_{His-10}$ was mobile and exhibited diffusion that was interrupted occasionally by periods during which it was nearly stationary (Movie 2, Fig. 4 *a*). A representative trajectory for CFTR$_{His-10}$ is shown in Fig. 4 *b*, in which the same confinement zone revisited by the particle at different times during the recording is indicated by the green and blue lines. This result is similar to those described previously for lipid rafts (27). Analysis of the functional relationship between the MSD and time indicates the type of motion present in the system (20). The MSD of the particle in Fig. 4 *a*, outside of the confinement zones, results in a linear profile indicative of Brownian motion (Fig. 4 *c*). However, the MSD of the particle when its motion is constrained results in a

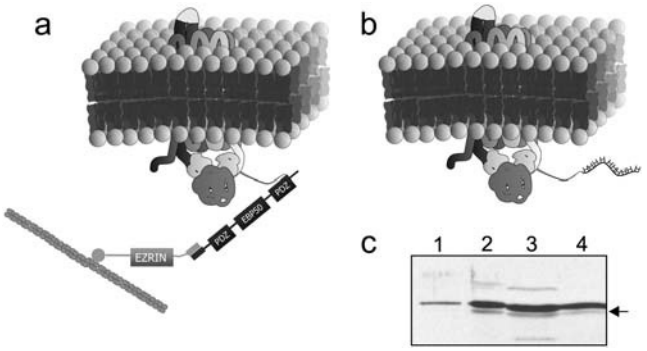

FIGURE 3 (*a*) Schematic of the EBP50/NHERF1 interaction with the PDZ domain binding motif at the C-terminus of CFTR, which is masked (*b*) by the addition of the decahistidine tag. (*c*) Western blot of an avidin pulldown of biotinylated CFTR. CFTR and $CFTR_{His\text{-}10}$ were enzymatically biotinylated, pulled down on avidin beads, and analyzed by Western blotting with anti-NHERF1 antibody. Lane 1, pulldown of $CFTR_{His\text{-}10}$ expressed in BHK cells; lane 2, pulldown using CFTR-expressing BHK cells. Lanes 3 and 4 show the protein in crude lysates obtained using cells that express $CFTR_{His\text{-}10}$ or CFTR, respectively. The solid arrow represents the molecular mass marker at 47.5 kDa.

plateau characteristic of confinement (Fig. 4 *d*). The MSD versus time was plotted for an ensemble of trajectories of quantum dot $CFTR_{His\text{-}10}$ complexes and a plateau was consistently obtained, indicating there is confined diffusion of the $CFTR_{His\text{-}10}$ complex (Fig. 4 *e*). Analysis of the trajectories outside of the transient confinement zones yielded a diffusion coefficient of $3.0 \pm 1.0 \times 10^{-2}\ \mu m^2 s^{-1}$ (Fig. 4 *c*). This value is ~2-fold greater than the diffusion coefficient obtained using FRAP, which measures an overall ensemble value for the freely diffusing and transiently confined populations. Most wild-type CFTR trajectories could not be analyzed for a diffusion coefficient using the MSD because there wasn't sufficient movement away from the origin.

We compared the SPT data of $CFTR_{His\text{-}10}$ with those obtained by ICS measurement of cells labeled with a much smaller streptavidin-dye CFTR conjugate by reanalyzing the same images used for SPT using ICS, a method that has not been applied previously to proteins labeled with quantum dots (Fig. 4 *f*). ICS analysis yielded very low noise autocorrelation curves, and Fig. 4 *f* shows a typical example with a calculated diffusion coefficient of $D = 3.7 \pm 1.1 \times 10^{-3}\ \mu m^2 s^{-1}$, very similar to the value determined for Streptavidin-Alexa 568 by ICS. The close agreement between results obtained for dye and quantum dot conjugates indicates that attaching the nanoparticle to CFTR had a negligible impact on its lateral mobility in the membrane, as has been reported previously for glycine receptors (25).

Fluorescence correlation spectroscopy of CFTR containing endosomes

CFTR undergoes endocytosis in BHK cells and is continuously recycled to the membrane (24). We minimized the contribution of fluorescent CFTR within endosomes by limiting measurement to the first 5–30 min after labeling cells for only 3–5 min on ice and by excluding from the analysis any particles that diffused out of the focal plane (since these were more likely to be internalized complexes). To further assess whether endosomes containing labeled CFTR could confound the SPT measurements, FCS was used to investigate the diffusion of CFTR in endosomes near the membrane. FCS can be used to measure the mobility and dynamics of labeled molecules in live cells and has been used to measure vesicle movements in the endocytic pathway (28).

After enzymatic biotinylation and labeling with Streptavidin-Alexa 488, the confocal volume used for FCS was focused on the membrane in a region over the nucleus (Fig. 5 *a*). Steady-state FCS measurements on the cell membrane resulted in bleaching of the membrane component, as characterized by a decrease in the count rate (Fig. 5 *d*, *inset*). Bleaching is observed when the fluorophore exhibits a long residence time (>1 s) in the FCS illumination volume, and thus is a result of low mobility in the membrane ($<10^{-2}\ \mu m^2 s^{-1}$) (28). In the case of CFTR, this means that the FCS focal volume includes a portion of the membrane (Fig. 5 *b*) containing slowly diffusing, plasma membrane-localized CFTR that is bleached. The relatively mobile endocytic vesicles containing CFTR remain unbleached and give rise to the autocorrelation curve, which includes the last 3–4 10-s repetitions of the count rate trace (Fig. 5 *d*). The recovered characteristic diffusion time was 33 ± 8 ms, corresponding to an average D of $1.7 \pm 0.5 \times 10^{-1}\ \mu m^2 s^{-1}$ and, not surprisingly, these vesicular diffusion times were virtually identical for both CFTR and $CFTR_{His\text{-}10}$. Using the Stokes-Einstein equation and assuming a cytosolic viscosity of $\eta \approx 5$ cP (28), the hydrodynamic diameter of the vesicles is ~450 nm. This size is larger than expected for clathrin-dependent endocytic vesicles (29), which are thought to average ~120 nm, and is most likely due to larger vesicle aggregates or tubules, which would dominate the autocorrelation curve as found previously in FCS studies of endosomes (28). Regardless, these diffusion coefficients are still an order of magnitude larger than those measured by SPT, indicating that the single particles tracked in our experiments were cell surface CFTR and unlikely to be in endocytic vesicles.

Cross-linking of CFTR by streptavidin

Cross-linking membrane proteins may slow their diffusion by a factor of up to five, depending on the protein and cell type (30). Streptavidin is a tetrameric protein, capable of binding four biotin groups; consequently the streptavidin fluorophore label could potentially cross-link up to four CFTR molecules. To investigate the degree of cross-linking, CFTR was biotinylated on live cells, streptavidin was bound, and the cell lysate was run on an 8% SDS-PAGE gel and probed using anti-streptavidin (Fig. 1 *e*). The Western blot shows two distinct bands corresponding to monomeric

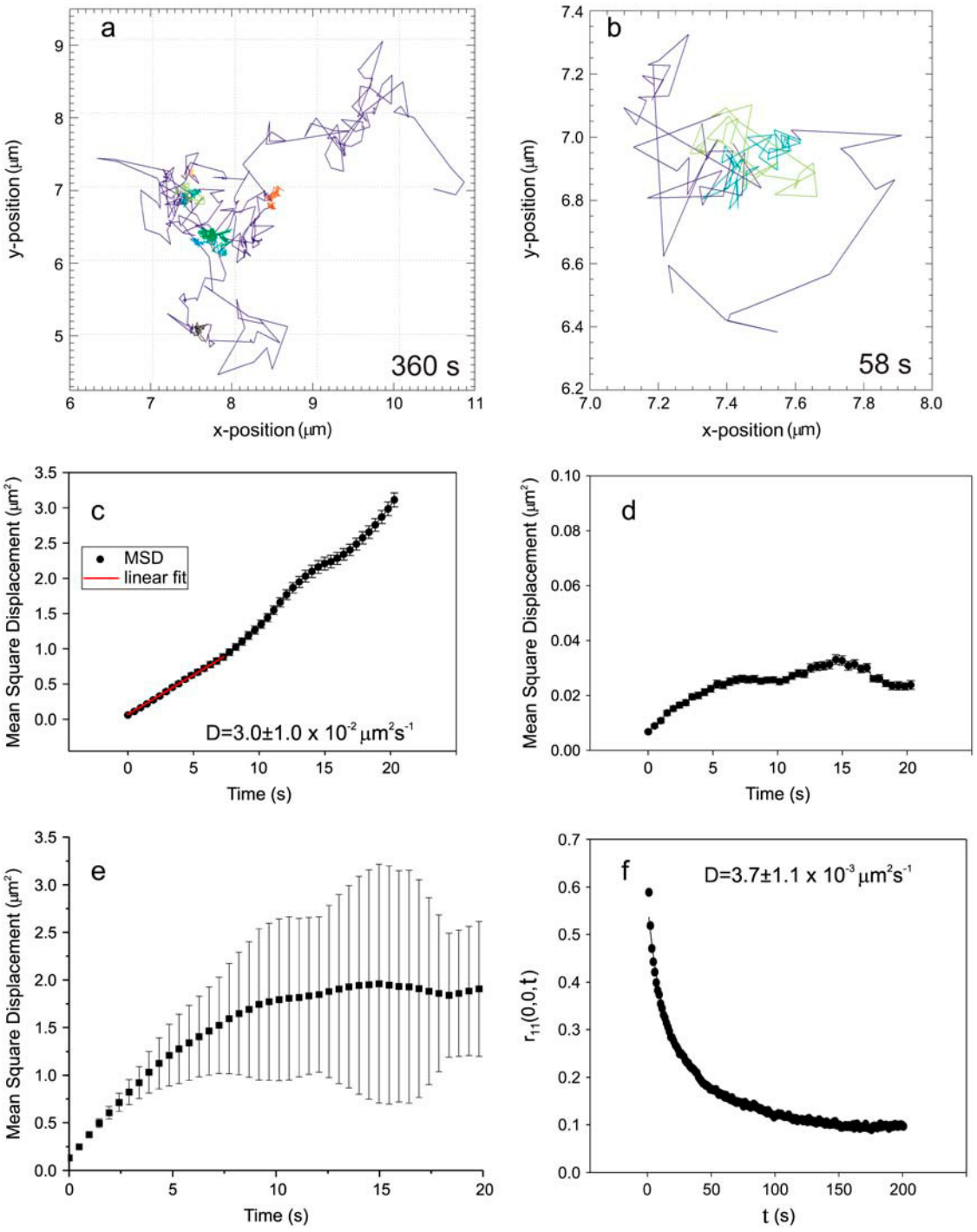

FIGURE 4 SPT and ICS of $CFTR_{His\text{-}10}$ labeled with quantum dots (QD) after enzymatic biotinylation. (*a*) Example of a QD trajectory obtained by analysis of an LSM image time series consisting of 743 time steps collected over 360 s. The colored tracks indicate regions of confinement. (*b*) Higher zoom portion of the trajectory from (*a*) which shows the revisitation of confinement zones (frames 350–470, time sampling of 0.483 s/frame). MSD as a function of time for regions outside of confinement zones (*c*) and within confinement zones (*d*) for the particle tracked in (*a*). The measured *D* from the analysis of MSD versus time curves was $3.0 \pm 1.0 \times 10^{-2}\ \mu m^2 s^{-1}$. (*e*) MSD as a function of time calculated for an ensemble of trajectories ($N = 32$). (*f*) Normalized temporal intensity fluctuation autocorrelation function measured from a cell labeled with $CFTR_{His\text{-}10}$/QD. The *D* is determined from the best parameters for a 2D diffusion decay model (*solid line*).

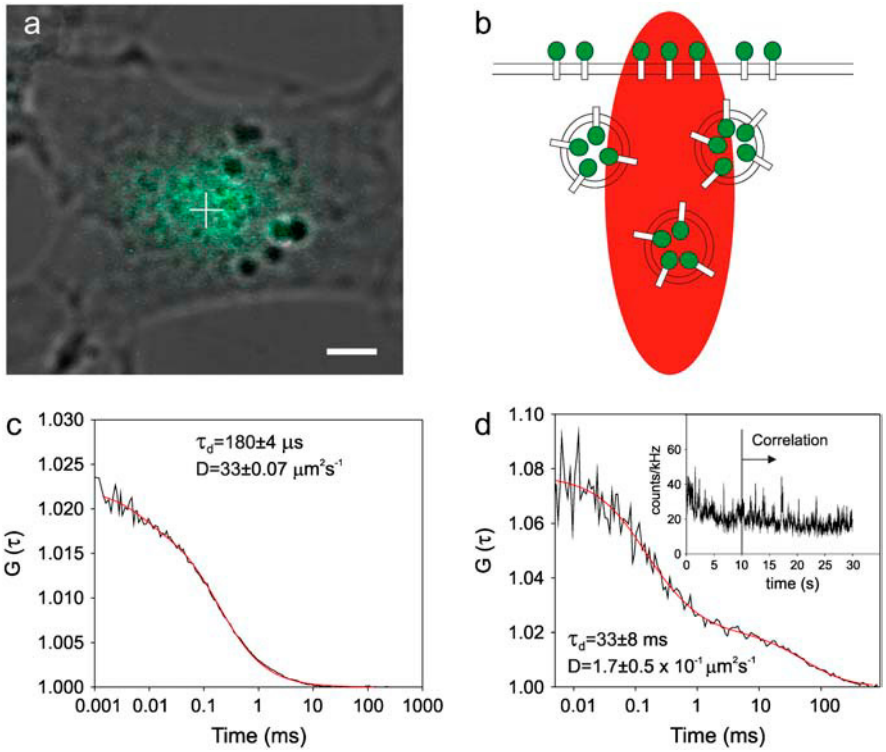

FIGURE 5 Enzymatically biotinylated CFTR labeled with Streptavidin-Alexa 488. (*a*) Laser scanning microscope image of the apical membrane of BHK cells with labeled CFTR-biotintag and the location of the confocor focus (cross-hair). Scale bar, 5 μm. (*b*) Illustration showing the FCS illumination volume positioned on the apical membrane where CFTR in the plasma membrane and in endocytic vesicles is detected. (*c*) Autocorrelation curves of free Streptavidin-Alexa 488 in solution. (*d*) Average autocorrelation curve of the last 4 $\times$ 10 s intervals of the FCS measurement. The first 10 s of the count rate decayed sharply during the measurement, consistent with the bleaching of the slowly moving CFTR in the membrane.

CFTR (running at 175 kDa as Band C, the mature form) and dimerized CFTR (running at 350 kDa, indicating a dimer of Band C). This demonstrates labeling of mature CFTR at the cell surface and suggests that streptavidin can cross-link CFTR into stable dimers. Although the oligomeric state of CFTR remains controversial, cross-linking of CFTR into dimers is consistent with the existence of stable, naturally occurring dimers at the cell surface as reported and quantified in Chinese hamster ovary (CHO) and T_{84} cells by size exclusion chromatography and nondissociative gel electrophoresis (23) and observed in freeze fracture electron micrographs (31) and low-resolution structures (R. Ford, The University of Manchester, personal communication, 2006). Since the relative amounts of cross-linked dimer are similar to those reported previously (23), the mobilities observed in this study are consistent with the naturally occurring oligomeric state of the protein independent of streptavidin cross-linking.

In addition to the issue of the tetrameric streptavidin binding, the SPT experiments could be complicated by the fact that each qDot is coated with 2–3 streptavidin molecules. It has previously been determined that a 10-fold excess of biotin will block streptavidin:qDot binding (32), and this was confirmed in our experimental system. To have adequate binding with minimal cross-linking, a fivefold excess of free biotin was routinely added during the labeling step. Moreover, ICS studies of qDot-labeled CFTR yielded a diffusion coefficient that was similar in magnitude to that measured using a smaller streptavidin fluorophore label.

Simulations comparing FRAP, ICS, and SPT measurements under identical conditions

Diffusion coefficients of $CFTR_{His\text{-}10}$ obtained using FRAP in this work and in a previous study of GFP-CFTR (9) were ~4-fold faster than those measured using ICS. The SPT results were ~2-fold faster than the FRAP results, due to the fact that the D was determined using the MSD of CFTR when it is outside of the confinement zones. We hypothesized that the differences between ICS and FRAP measurements may be found in the way in which these two techniques are influenced by the transiently confined $CFTR_{His\text{-}10}$ population that was observed in SPT. To better understand how such confinement contributes to the calculated D, we carried out computer simulations of laser scanning microscopy time series imaging of point emitters in a 2D plane while systematically varying the microscopy collection parameters and mobility properties of the particles. The simulations modeled 128 $\times$ 128 pixel images, with 0.1 μm/pixel and 100 images per time series to match the conditions used during experiments on live cells. Image time steps of 1 and 4 s were used, as during the ICS and FRAP experiments, respectively. Simulations were generated to model the experimental conditions as accurately as possible, with a random distribution of 200-nm diameter domains in the 2D plane, representing the confinement regions (Fig. 6 *b*) (22). Diffusion coefficients were set for the inside and outside of the domains (D_{in} and D_{out}) and the probabilities assigned for entering and exiting the domains (P_{in} and P_{out}, respectively). In the simulation, when a particle encounters a domain the P_{in}

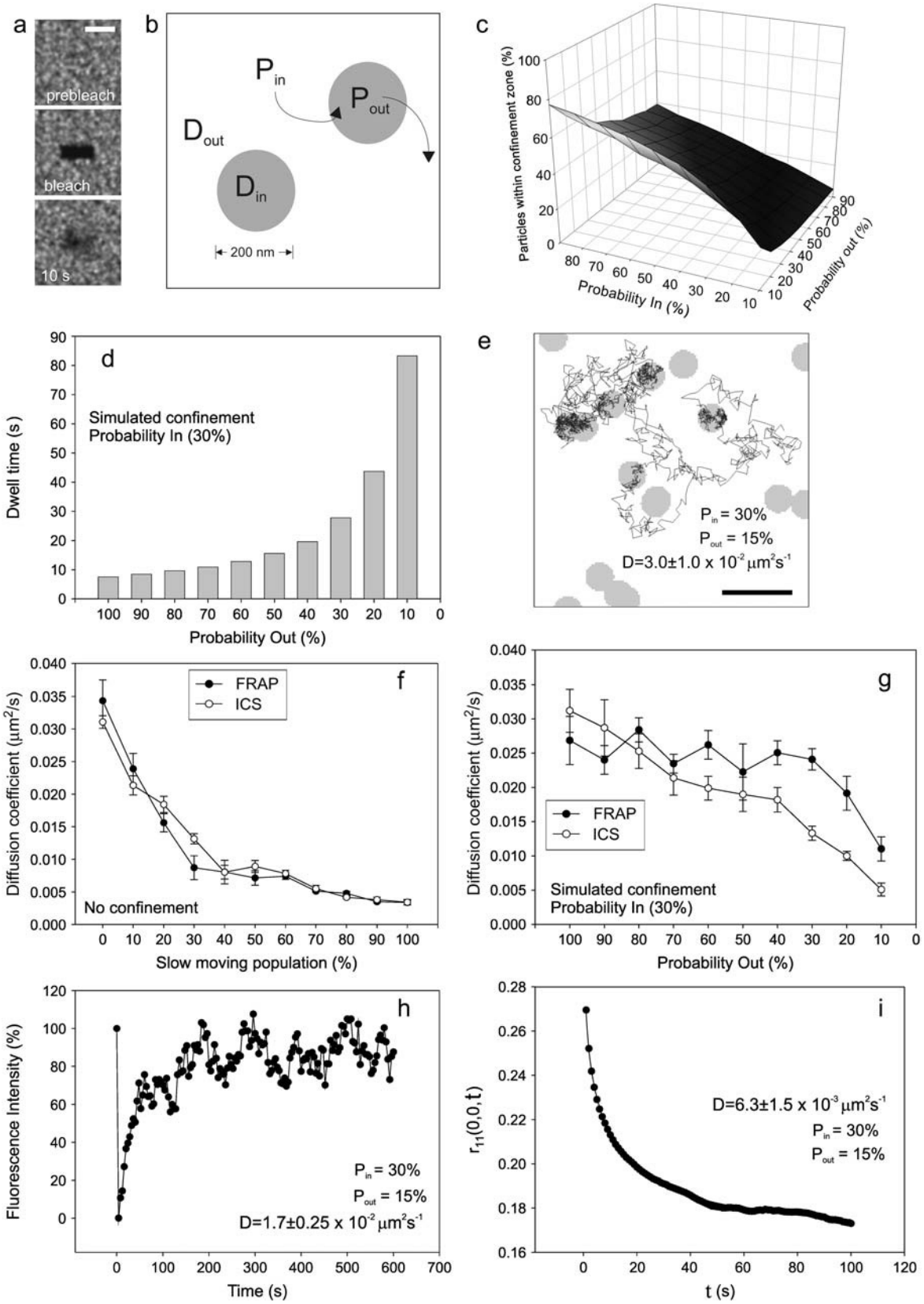

FIGURE 6 Imaging simulations of freely diffusing and transiently confined point particles and the results of FRAP and ICS lateral mobility measurements. (*a*) Images from a simulated FRAP experiment. Bleach box, 5 μm. Scale bar, 5 μm. (*b*) Scheme for simulating transient confinement, where P_{in} and P_{out} represent the probability of entering and exiting a domain, and D_{in} and D_{out} represent the diffusion coefficient inside and outside the domain, respectively. The

value determines the probability of entering, whereas the P_{out} value determines the probability of exiting after encountering the domain perimeter from inside a domain (22). For the subsequent simulations, a D_{out} of 3.0×10^{-2} $\mu m^2 s^{-1}$ was used (representing the D determined experimentally by SPT outside the domains) and a D_{in} of 3.0×10^{-3} $\mu m^2 s^{-1}$ (a 10-fold slower rate for within the domains). A three-dimensional (3D) plot illustrates the effect of varying both P_{in} and P_{out}, with an increase in the P_{in} and decrease in P_{out} leading to an overall increase in particle confinement (Fig. 6 *c*). When the P_{in} was set to 30%, the confinement zone dwell time increased as the P_{out} was decreased (Fig. 6 *d*). At the single particle level, these parameters resulted in 30% of the population residing within the confinement zones and a mean-zone dwell time of 44 s, values that were very similar to those determined experimentally by SPT. Fig. 6 *e* shows that these parameters, when used to simulate SPT of qDot-CFTR, yielded trajectories remarkably similar to those obtained experimentally (compare with Fig. 4 *a*).

Interestingly, the effect of these transient confinement domains on the diffusion coefficients determined by FRAP and ICS analysis was quite different. When simulating two populations of unconfined particles, one with a D set to be the same as that measured by SPT for particles outside of the domains (3.0×10^{-2} $\mu m^2 s^{-1}$) and another diffusing an order of magnitude slower (3.0×10^{-3} $\mu m^2 s^{-1}$), both ICS and FRAP show a similar decrease in the measured D as the fraction of the slower (but unconfined diffusers) was increased (Fig. 6 *f*). If, however, confinement was included in the simulation using the same diffusion coefficients but varying P_{out}, the apparent D obtained by ICS measurement declined more rapidly compared to FRAP as the P_{out} was decreased (Fig. 6 *g*). The most accurate match to the experimental results was obtained when P_{in} was 30% and P_{out} was equal to 15%. The apparent diffusion coefficients measured by ICS and FRAP in this case were $6.3 \pm 1.5 \times 10^{-3}$ $\mu m^2 s^{-1}$ and $1.7 \pm 0.25 \times 10^{-2}$ $\mu m^2 s^{-1}$, respectively (Fig. 6, *h* and *i*), illustrating the differential effect of transient confinement on the D using these two techniques.

DISCUSSION

Lateral mobility of wild-type CFTR depends on interactions with PDZ domain proteins

CFTR interacts with many different proteins; however, the functional consequences of those associations are not well understood and it remains uncertain if they lead to stable complexes. Interactions with scaffolding proteins and the actin cytoskeleton may regulate CFTR channel activity directly and also by tethering various regulatory molecules.

We hypothesized that interaction of wild-type CFTR with PDZ domain proteins would reduce its lateral mobility. Although a previous FRAP study did not observe an immobilized population of GFP-CFTR at the cell surface (9), we found using three different methods that >50% of the wild-type CFTR on BHK cells is immobile. BHK cells overexpress CFTR at high levels and there may be a limited supply of PDZ domain proteins available for binding; therefore, it is conceivable that the immobile fraction would be higher in cells expressing CFTR at physiological levels. Since CFTR mobility may depend on expression level and other factors such as cell type (epithelial versus nonepithelial) and the extent of differentiation and apical-basolateral polarization, further studies of CFTR diffusion in polarized epithelial cells are needed.

Adding a decahistidine tag at the C-terminus of CFTR to disrupt the binding of PDZ domain proteins reduced the immobile fraction and increased the diffusion coefficient significantly. Thus PDZ domain proteins have a major influence on CFTR mobility in BHK cells. Although the large immobile fraction precluded calculation of a diffusion coefficient for wild-type CFTR using FRAP, the value obtained by ICS indicated that it was exceedingly low, and this was confirmed by tracking single qDots bound to CFTR. By contrast, $CFTR_{His\text{-}10}$ movements were rapid according to both FRAP and ICS.

Single particle tracking reveals intriguing dynamics after CFTR is released from PDZ domains

The behavior of $CFTR_{His\text{-}10}$ was very different from that of wild-type CFTR. Disrupting PDZ domain interactions led to rapid diffusion that was interrupted for periods lasting <1 min, during which time the quantum dot appeared to vibrate around one spot before being released. In some instances, quantum dots revisited the same spot several times, reminiscent of proteins that enter confinement zones or lipid rafts (33). The finding that CFTR and $CFTR_{His\text{-}10}$ have very different mobilities argues they were indeed at the cell surface, since it is unlikely that a polyhistidine tag on CFTR would accelerate vesicle movements beneath the plasma membrane. Moreover, control FCS experiments confirmed

FIGURE 6 (Continued).
domain diameter was 200 nm, and the number of domains used was 120 in a 128 × 128 pixel region. (*c*) 3D mesh graph showing the percentage confinement as a function of P_{in} and P_{out}. (*d*) Dwell times within confinement zones as P_{out} is decreased with P_{in} set at 30%. (*e*) Simulation of an SPT experiment showing transient confinement similar to that observed during the SPT experiment shown in Fig. 4 *a*. ($D_{in} = 3.0 \times 10^{-3}$ $\mu m^2 s^{-1}$, $D_{out} = 3.0 \times 10^{-2}$ $\mu m^2 s^{-1}$, $P_{in} =$ 30%, $P_{out} = 15\%$, total time = 360 s). Scale bar, 0.5 μm. (*f*) ICS and FRAP measured diffusion coefficients for simulations of two diffusing populations with no confinement ($D_{slow} = 3.0 \times 10^{-3}$ $\mu m^2 s^{-1}$, $D_{fast} = 3.0 \times 10^{-2}$ $\mu m^2 s^{-1}$), as a function of the fraction of the slower diffusing population. (*g*) ICS and FRAP measured diffusion coefficients for simulations with transient confinement showing the effect of increasing P_{out}. (*h*) FRAP recovery kinetics of a simulated confinement experiment using the same parameters as in *e*. (*i*) ICS autocorrelation function of a simulated confinement experiment using the same parameters as in *e*.

that the observed particles were not in endosomes, which have diffusion coefficients that are an order of magnitude faster than those for CFTR in the lipid bilayer.

We conclude from these studies that most CFTR on BHK cells is tethered through PDZ domain proteins and appears immobilized when studied on a timescale of minutes. PDZ domain interactions with the C-terminus probably influence CFTR mobility (9) through mechanisms similar to those of other ion channels and receptors (34,35). PDZ domain-containing proteins cluster and immobilize K channels (36), and studies of AMPA receptors indicate that such interactions may also be regulated physiologically (37). In T cells, protein-protein interactions induced by the formation of complexes and microdomains have recently been shown to cause diffusional trapping that facilitates cell signaling (38). Transient interactions of CFTR with other proteins or lipid domains become apparent when PDZ interactions are disrupted and diffusing CFTR molecules enter transient confinement zones. The biochemical basis of confinement remains to be investigated and may involve multiple lipid- and protein-dependent mechanisms (27). In this regard, it is interesting that CFTR has been found to associate with lipid microdomains at regions of *P. aeruginosa* infection (39).

Comparison with previous studies of CFTR mobility

Studies of a GFP-CFTR fusion protein revealed rapid diffusion in the endoplasmic reticulum (diffusion coefficient 10^{-1} $\mu m^2 s^{-1}$ (40)) and a diffusion coefficient of 10^{-2} $\mu m^2 s^{-1}$ in the plasma membrane, similar to FRAP results obtained for $CFTR_{His\text{-}10}$ in this study ($1.4 \pm 0.6 \times 10^{-2}$ $\mu m^2 s^{-1}$). However, a major difference between the studies was the immobile fraction, which was negligible for GFP-CFTR (40) but >50% for wild-type CFTR in this study, and 28% and 23% for $CFTR_{His\text{-}10}$ using ICS and FRAP, respectively. The difference may be due in part to butyrate, which was used in the previous study to elevate GFP-CFTR expression (41); however, this is probably not the entire explanation since a large immobile fraction was observed in BHK cells, which have very high CFTR expression. The unpolarized Madin Darby canine kidney cells used previously may contain different interacting proteins compared to the BHK cells. Alternatively, fusion of GFP to the amino terminus of CFTR may disrupt protein interactions that normally immobilize CFTR. We found that the diffusion coefficient obtained by FRAP is relatively insensitive to confinement; therefore, loss of the immobile fraction might not noticeably affect the diffusion coefficient calculated using this technique.

Comparison of three methods for measuring lateral mobility

In addition to revealing new features of CFTR movement at the cell surface, these results demonstrate the usefulness of external biotinylation target sequences for quantitative studies of membrane proteins. To visualize CFTR movements on the cell surface, a biotinylation target sequence was inserted into the fourth extracellular loop of CFTR so that fluorescent streptavidin conjugates could be specifically bound. This method has some advantages over other methods: the affinity of the biotin-streptavidin interaction ($K_d = 10^{-13}$ M) exceeds that between an antibody and its epitope (42), and streptavidin is smaller than IgG (60 kDa versus 150 kDa). We used streptavidin conjugates of Alexa 488 and Alexa 568 for FRAP and ICS, respectively, and streptavidin conjugated quantum dots for SPT and ICS, but it should be possible to attach other probes to CFTR and to other membrane proteins that tolerate insertion of a small extracellular peptide.

These results also provide, to our knowledge, the first comparison of mobility estimates obtained by FRAP, ICS, and SPT under the same experimental conditions. The results suggest that the diffusion coefficients calculated for $CFTR_{His\text{-}10}$ using ICS are more strongly influenced by transient confinement than those determined by FRAP, probably because fluorescence recovery curves are dominated by the more abundant and rapidly diffusing species during FRAP, obscuring the confinement. This study also expands the proven applications for quantum dots, which are an exciting alternative to fluorescent dyes due to their photostability and intense emission (43) but which have not been used previously for ICS studies. We calculated similar diffusion coefficients for CFTR labeled with fluorescent dyes or quantum dots, and consistent values were obtained when the images were analyzed using ICS and SPT. Thus quantum dots provide a convenient tool for combining complementary ensemble and single molecule methods.

ICS is an ensemble method for studying membrane protein dynamics in time and space which can quantify membrane receptor diffusion, lateral flow, and the immobile fraction. It has been used successfully to characterize integrin dynamics and their interactions with other proteins and to determine diffusion coefficients and velocity vectors for directed flow of membrane-associated macromolecules (19,44). Similar diffusion coefficients for CFTR were obtained by ICS when streptavidin-dye or streptavidin-quantum dot conjugates were used, suggesting the size of the quantum dot has little impact on the lateral mobility of membrane macromolecules, a conclusion that is consistent with previous studies of membrane proteins (25).

The apparent diffusion coefficient of $CFTR_{His\text{-}10}$ measured by FRAP was higher than that obtained using ICS. Srivastava and Petersen (45) found a similar discrepancy for transferrin receptors and attributed the lower ICS D value to slow diffusion of receptor clusters, which are brighter and therefore dominate the autocorrelation function. However, when a heterogeneous population of slow-moving bright particles (representing CFTR clusters) and fast-moving dim particles (monomers) was simulated, we found that the

measured diffusion coefficients declined similarly for FRAP and ICS as the fraction of slow species was increased (data not shown). Therefore $CFTR_{His\text{-}10}$ clustering is unlikely to explain the apparent discrepancy between diffusion coefficients obtained by these two methods. An alternative explanation was suggested by SPT results obtained with $CFTR_{His\text{-}10}$, which revealed zones of transient confinement. When this behavior was studied in silico, transient confinement resulted in a lower ICS measured diffusion coefficient, but had less effect on the *D* value calculated using FRAP despite contributing to the immobile fraction for both methods.

Transient confinement similar to that reported here for $CFTR_{His\text{-}10}$ may contribute to the immobile fraction observed when other proteins are studied using FRAP (46,47). Our results suggest that transient confinement of membrane receptors can be detected by comparing the results obtained using FRAP and ICS. Further studies should examine whether the chloride channel activity of CFTR is affected by its entry into transient confinement zones.

SUPPLEMENTARY MATERIAL

An online supplement to this article can be found by visiting BJ Online at http://www.biophysj.org.

We thank Jacynthe LaLiberté for help with preliminary imaging experiments.

This work was supported by grants from the Canadian CF Foundation, CF Foundation (USA), and National Institutes of Health (National Institute of Diabetes and Digestive and Kidney Diseases) to J.W.H., and the Natural Sciences and Engineering Research Council (Canada) and Canada Foundation for Innovation to P.W.W. J.W.H. was a senior scientist of the Canadian Institutes of Health Research (CIHR). I.R.B. was the recipient of a Canadian Institute of Health Research (CIHR) fellowship. B.H. and D.L.K. acknowledge Natural Sciences and Engineering Research Council of Canada graduate fellowships.

REFERENCES

1. Riordan, J. R., J. M. Rommens, B. Kerem, N. Alon, R. Rozmahel, Z. Grzelczak, J. Zielenski, S. Lok, N. Plaversusic, and J. L. Chou. 1989. Identification of the cystic fibrosis gene: cloning and characterization of complementary DNA. *Science*. 245:1066–1073.
2. Voltz, J. W., E. J. Weinman, and S. Shenolikar. 2001. Expanding the role of NHERF, a PDZ-domain containing protein adapter, to growth regulation. *Oncogene*. 20:6309–6314.
3. Li, C., K. Roy, K. Dandridge, and A. P. Naren. 2004. Molecular assembly of cystic fibrosis transmembrane conductance regulator in plasma membrane. *J. Biol. Chem.* 279:24673–24684.
4. Milewski, M. I., J. E. Mickle, J. K. Forrest, D. M. Stafford, B. D. Moyer, J. Cheng, W. B. Guggino, B. A. Stanton, and G. R. Cutting. 2001. A PDZ-binding motif is essential but not sufficient to localize the C terminus of CFTR to the apical membrane. *J. Cell Sci.* 114:719–726.
5. Raghuram, V., D. D. Mak, and J. K. Foskett. 2001. Regulation of cystic fibrosis transmembrane conductance regulator single-channel gating by bivalent PDZ-domain-mediated interaction. *Proc. Natl. Acad. Sci. USA*. 98:1300–1305.
6. Naren, A. P., M. W. Quick, J. F. Collawn, D. J. Nelson, and K. L. Kirk. 1998. Syntaxin 1A inhibits CFTR chloride channels by means of domain-specific protein-protein interactions. *Proc. Natl. Acad. Sci. USA*. 95:10972–10977.
7. Sun, F., M. J. Hug, C. M. Lewarchik, C. H. Yun, N. A. Bradbury, and R. A. Frizzell. 2000. E3KARP mediates the association of ezrin and protein kinase A with the cystic fibrosis transmembrane conductance regulator in airway cells. *J. Biol. Chem.* 275:29539–29546.
8. Schwiebert, E. M., D. J. Benos, M. E. Egan, M. J. Stutts, and W. B. Guggino. 1999. CFTR is a conductance regulator as well as a chloride channel. *Physiol. Rev.* 79:S145–S166.
9. Haggie, P. M., B. A. Stanton, and A. S. Verkman. 2004. Increased diffusional mobility of CFTR at the plasma membrane after deletion of its C-terminal PDZ binding motif. *J. Biol. Chem.* 279:5494–5500.
10. Haggie, P. M., B. A. Stanton, and A. S. Verkman. 2002. Diffusional mobility of the cystic fibrosis transmembrane conductance regulator mutant, delta F508-CFTR, in the endoplasmic reticulum measured by photobleaching of GFP-CFTR chimeras. *J. Biol. Chem.* 277:16419–16425.
11. Lippincott-Schwartz, J., E. Snapp, and A. Kenworthy. 2001. Studying protein dynamics in living cells. *Nat. Rev. Mol. Cell Biol.* 2:444–456.
12. Wiseman, P. W., J. A. Squier, M. H. Ellisman, and K. R. Wilson. 2000. Two-photon image correlation spectroscopy and image cross-correlation spectroscopy. *J. Microsc.* 200:14–25.
13. Schatz, P. J. 1993. Use of peptide libraries to map the substrate specificity of a peptide-modifying enzyme: a 13 residue consensus peptide specifies biotinylation in Escherichia coli. *Biotechnology (N. Y.).* 11:1138–1143.
14. Schultz, B. D., A. Takahashi, C. Liu, R. A. Frizzell, and M. Howard. 1997. FLAG epitope positioned in an external loop preserves normal biophysical properties of CFTR. *Am. J. Physiol.* 273:C2080–C2089.
15. Chang, X. B., J. A. Tabcharani, Y. X. Hou, T. J. Jensen, N. Kartner, N. Alon, J. W. Hanrahan, and J. R. Riordan. 1993. Protein kinase A (PKA) still activates CFTR chloride channel after mutagenesis of all 10 PKA consensus phosphorylation sites. *J. Biol. Chem.* 268:11304–11311.
16. Cull, M. G., and P. J. Schatz. 2000. Biotinylation of proteins in vivo and in vitro using small peptide tags. *Methods Enzymol.* 326:430–440.
17. Siggia, E. D., J. Lippincott-Schwartz, and S. Bekiranov. 2000. Diffusion in inhomogeneous media: theory and simulations applied to whole cell photobleach recovery. *Biophys. J.* 79:1761–1770.
18. Ellenberg, J., E. D. Siggia, J. E. Moreira, C. L. Smith, J. F. Presley, H. J. Worman, and J. Lippincott-Schwartz. 1997. Nuclear membrane dynamics and reassembly in living cells: targeting of an inner nuclear membrane protein in interphase and mitosis. *J. Cell Biol.* 138:1193–1206.
19. Wiseman, P. W., C. M. Brown, D. J. Webb, B. Hebert, N. L. Johnson, J. A. Squier, M. H. Ellisman, and A. F. Horwitz. 2004. Spatial mapping of integrin interactions and dynamics during cell migration by image correlation microscopy. *J. Cell Sci.* 117:5521–5534.
20. Saxton, M. J., and K. Jacobson. 1997. Single-particle tracking: applications to membrane dynamics. *Annu. Rev. Biophys. Biomol. Struct.* 26:373–399.
21. Simson, R., E. D. Sheets, and K. Jacobson. 1995. Detection of temporary lateral confinement of membrane proteins using single-particle tracking analysis. *Biophys. J.* 69:989–993.
22. Wawrezinieck, L., H. Rigneault, D. Marguet, and P. F. Lenne. 2005. Fluorescence correlation spectroscopy diffusion laws to probe the submicron cell membrane organization. *Biophys. J.* 89:4029–4042.
23. Ramjeesingh, M., J. F. Kidd, L. J. Huan, Y. Wang, and C. E. Bear. 2003. Dimeric cystic fibrosis transmembrane conductance regulator exists in the plasma membrane. *Biochem. J.* 374:793–797.
24. Lukacs, G. L., G. Segal, N. Kartner, S. Grinstein, and F. Zhang. 1997. Constitutive internalization of cystic fibrosis transmembrane conductance regulator occurs via clathrin-dependent endocytosis and is regulated by protein phosphorylation. *Biochem. J.* 328:353–361.
25. Dahan, M., S. Levi, C. Luccardini, P. Rostaing, B. Riveau, and A. Triller. 2003. Diffusion dynamics of glycine receptors revealed by single-quantum dot tracking. *Science*. 302:442–445.
26. Chan, W. C., and S. Nie. 1998. Quantum dot bioconjugates for ultrasensitive nonisotopic detection. *Science*. 281:2016–2018.

27. Dietrich, C., B. Yang, T. Fujiwara, A. Kusumi, and K. Jacobson. 2002. Relationship of lipid rafts to transient confinement zones detected by single particle tracking. *Biophys. J.* 82:274–284.

28. Bacia, K., I. V. Majoul, and P. Schwille. 2002. Probing the endocytic pathway in live cells using dual-color fluorescence cross-correlation analysis. *Biophys. J.* 83:1184–1193.

29. Conner, S. D., and S. L. Schmid. 2003. Regulated portals of entry into the cell. *Nature.* 422:37–44.

30. Kusumi, A., C. Nakada, K. Ritchie, K. Murase, K. Suzuki, H. Murakoshi, R. S. Kasai, J. Kondo, and T. Fujiwara. 2005. Paradigm shift of the plasma membrane concept from the two-dimensional continuum fluid to the partitioned fluid: high-speed single-molecule tracking of membrane molecules. *Annu. Rev. Biophys. Biomol. Struct.* 34:351–378.

31. Eskandari, S., E. M. Wright, M. Kreman, D. M. Starace, and G. A. Zampighi. 1998. Structural analysis of cloned plasma membrane proteins by freeze-fracture electron microscopy. *Proc. Natl. Acad. Sci. USA.* 95:11235–11240.

32. Swift, J. L., R. Heuff, and D. T. Cramb. 2006. A two-photon excitation fluorescence cross-correlation assay for a model ligand-receptor binding system using quantum dots. *Biophys. J.* 90:1396–1410.

33. Chen, Y., B. Yang, and K. Jacobson. 2004. Transient confinement zones: a type of lipid raft? *Lipids.* 39:1115–1119.

34. Meier, J., C. Vannier, A. Sergé, A. Triller, and D. Choquet. 2001. Fast and reversible trapping of surface glycine receptors by gephyrin. *Nat. Neurosci.* 4:253–260.

35. Tardin, C., L. Cognet, C. Bats, B. Luonis, and D. Choquet. 2003. Direct imaging of lateral movements of AMPA receptors inside synapses. *EMBO J.* 22:4656–4665.

36. Burke, N. A., K. Takimoto, D. Li, W. Han, S. C. Watkins, and E. S. Levitan. 1999. Distinct structural requirements for clustering and immobilization of K^+ channels by PSD-95. *J. Gen. Physiol.* 113:71–80.

37. Borgdorff, A. J., and D. Choquet. 2002. Regulation of AMPA receptor lateral movements. *Nature.* 417:649–653.

38. Douglass, A. D., and R. D. Vale. 2005. Single-molecule microscopy reveals plasma membrane microdomains created by protein-protein networks that exclude or trap signaling molecules in T cells. *Cell.* 121:937–950.

39. Kowalski, M. P., and G. B. Pier. 2004. Localization of cystic fibrosis transmembrane conductance regulator to lipid rafts of epithelial cells is required for Pseudomonas aeruginosa-induced cellular activation. *J. Immunol.* 172:418–425.

40. Haggie, P. M., B. A. Stanton, and A. S. Verkman. 2002. Diffusional mobility of the cystic fibrosis transmembrane conductance regulator mutant, ΔF508-CFTR, in the endoplasmic reticulum measured by photobleaching of GFP-CFTR chimeras. *J. Biol. Chem.* 277:16419–16425.

41. Haggie, P. M., G. L. Lukacs, and A. S. Verkman. 2005. Tracking of quantum dot-labeled single CFTR molecules in plasma membrane of live cells. The Nineteenth Annual North American Cystic Fibrosis Conference. October 20–23, 2005.

42. Piran, U., and W. J. Riordan. 1990. Dissociation rate constant of the biotin-streptavidin complex. *J. Immunol. Methods.* 133:141–143.

43. Gao, X., L. Yang, J. A. Petros, F. F. Marshall, J. W. Simons, and S. Nie. 2005. In vivo molecular and cellular imaging with quantum dots. *Curr. Opin. Biotechnol.* 16:63–72.

44. Hebert, B., S. Costantino, and P. W. Wiseman. 2005. Spatiotemporal image correlation spectroscopy (STICS) theory, verification, and application to protein velocity mapping in living CHO cells. *Biophys. J.* 88:3601–3614.

45. Srivastava, M., and N. O. Petersen. 1998. Diffusion of transferrin receptor clusters. *Biophys. Chem.* 75:201–211.

46. Feder, T. J., I. Brust-Mascher, J. P. Slattery, B. Baird, and W. W. Webb. 1996. Constrained diffusion or immobile fraction on cell surfaces: a new interpretation. *Biophys. J.* 70:2767–2773.

47. Sheets, E. D., G. M. Lee, R. Simson, and K. Jacobson. 1997. Transient confinement of a glycosylphosphatidylinositol-anchored protein in the plasma membrane. *Biochemistry.* 36:12449–12458.

48. Zhu, T., D. Dahan, A. Evagelidis, S. Zheng, J. Luo, and J. W. Hanrahan. 1999. Association of cystic fibrosis transmembrane conductance regulator and protein phosphatase 2C. *J. Biol. Chem.* 274: 29102–29107.